Molecular Dynamics Study on the Effects of Chain Branching on the Physical Properties of Lipid Bilayers: 2. Permeability

Wataru Shinoda,*,† Masuhiro Mikami,† Teruhiko Baba,‡ and Masakatsu Hato‡

Research Institute for Computational Sciences (RICS), National Institute of Advanced Industrial Science and Technology (AIST), Central-2, Umezono 1-1-1, Tsukuba 305-8568, Japan, and Nanotechnology Research Institute (NRI), National Institute of Advanced Industrial Science and Technology (AIST), Central-5, Higashi 1-1-1, Tsukuba 305-8565, Japan

Received: July 11, 2003; In Final Form: April 21, 2004

We studied the effects of chain branching on the water and nonionic (neutral) solute permeability of lipid bilayers in a molecular dynamics simulation comparing two bilayers: dipalmitoylphosphatidylcholine (DPPC) and diphytanoylphosphatidylcholine (DPhPC). The calculated free energy profiles of several neutral solute and water molecules across the lipid membranes showed that chain branching caused no significant changes in the solubility of these molecules inside the membrane core. However, an analysis of the cavity distribution in each of these bilayer systems demonstrated that the branch-chained DPhPC bilayer had, compared with the straight-chained DPPC bilayer, a relatively small and discrete free volume distribution in the hydrophobic part. This suggests that small penetrants have a lower rate of diffusion inside branch-chained lipid bilayers. Actually, water molecules showed lower local diffusion coefficients inside the DPhPC membrane than inside the DPPC membrane. The low penetrant mobility of the former must correlate with the slower dynamics of the branched DPhPC chains. Thus, we conclude that chain branching effects on the permeability are, as far as neutral small penetrants are concerned, attributable mainly to the reduction of chain dynamics. The effects of chain branching on proton permeability are also discussed in the context of the proton-wire hypothesis.

1. Introduction

Lipid bilayers are one of the major structural elements of biological membranes. Because they are basically impermeable to ions and bulky molecules, lipid bilayers can maintain an osmotic gradient across the membrane and support selective transport of these molecules through membrane proteins. On the other hand, small uncharged molecules, such as those of water, ammonia, and carbon dioxide, do permeate across lipid bilayers at significant rates.[1,2] Furthermore, even small cations, especially protons, can leak through lipid membranes in substantial amounts.[2] Not surprisingly, the permeability of many cations and small neutral molecules is significantly affected not only by the molecular structure of the lipid but also by the physical state of the bilayer.[2−4]

Archaeal lipids bearing highly branched hydrophobic chains form stable bilayers, which generally have low permeability of ionic and nonionic solutes.[5,6] Because of its high structural stability and low rate of ion leakage, a bilayer composed of a synthetic model archaeal lipid, diphytanoylphosphatidylcholine (DPhPC), is a popular reconstitution matrix of channel-forming proteins.[7] Indeed, proton permeability measurements demonstrated that the bilayer formed by DPhPC molecules allowed less proton permeability than that formed by straight-chained lipids, such as egg yolk phosphatidylcholine, by a factor of ∼4 under equal thermodynamic conditions.[8] On the other hand, comparative water permeability measurements on DPhPC and straight-chained *Escherichia coli* lipid membranes suggested that chain branching does not significantly affect the water permeation rate,[5] although *E. coli* lipid membrane contains a large amount of unsaturated lipids, which contribute to the enhancement of the water permeability of bilayers.[9] This observation, furthermore, seems to be in conflict with a previous comparative study on water diffusion through hydrocarbon liquids, *n*-hexadecane and 2,6,10,15,19,23-hexamethyl tetracosane, in which it was found that chain branching reduced water diffusion by a factor of 2∼3.[10] Although almost all tentative explanations proposed for the effect of chain branching on water permeability have focused on steric hindrance ascribed to methyl branches, the detailed molecular mechanism underlying chain branching effect is still unclear.

In our preceding paper,[11] we used molecular dynamics simulations to observe that DPhPC chain has low chain mobility as a result of chain "entrapment" by the lateral neighboring lipids. The results suggested that these variations in bilayer properties would affect solute permeability. In the present paper, we focus on the effects of chain branching on the permeability of small neutral molecules across lipid bilayers, and we undertake a series of comparative simulations on the straight-chained dipalmitoylphosphatidylcholine (DPPC) and branch-chained DPhPC bilayers. For these two systems, first, the free energy profiles of several neutral penetrants along the bilayer normal were calculated by means of a particle insertion technique with a cavity-based sampling[12] of the molecular configurations generated by NPT-MD simulations; second, local diffusion coefficients of water along the bilayer normal as well as in the bilayer plane were calculated in order to elucidate how chain branching alters water mobility. Free volume distributions in the bilayer systems were also investigated to shed light on how chain branching changes the membrane-interior environ-

* To whom correspondence should be addressed. E-mail: w.shinoda@aist.go.jp. Phone: +81-29-861-6251. Fax: +81-29-851-5426.
† Research Institute for Computational Sciences.
‡ Nanotechnology Research Institute.

10.1021/jp035998+ CCC: $27.50
Published on Web 05/26/2004

TABLE 1: Interaction Parameters and Geometries for the Inserted Molecules

molecule	atom	ϵ [kcal/mol]	r_{min} [Å]	charge [e]	geometry[f]
H_2O[a]	O	0.1521	3.5364	−0.834	$r_{OH} = 0.9572$
	H	0.0460	0.4490	0.417	$\theta_{HOH} = 104.52$
NH_3[b]	N	0.2100	3.3450	−0.804	$r_{NH} = 1.012$
	H			0.268	$\theta_{HNH} = 106.7$
O_2[a]	O	0.1200	3.4000	0.000	$r_{OO} = 1.208$
CO[a]	C	0.1100	4.2000	0.021	$r_{CO} = 1.128$
	O	0.1200	3.4000	−0.021	
NO[c]	N	0.1700	3.6480	0.028	$r_{NO} = 1.150$
	O	0.1590	3.5020	−0.028	
CO_2[d]	C	0.1230	3.6610	0.663	$r_{CO} = 1.230$
	O	0.1940	3.3830	−0.3315	$\theta_{OCO} = 180.0$
$CHCl_3$[e]	CH	0.0800	4.2650	0.420	$r_{CCl} = 1.758$
	Cl	0.4000	3.8950	−0.140	$\theta_{ClCCl} = 111.3$

[a] The models were taken from the CHARMM library.[14] [b] The parameters were taken from ref. 17. [c] The parameters were taken from ref. 18. [d] The parameters were taken from ref. 19. [e] The parameters were taken from ref. 20, and CH was treated as the united atom in the model. [f] The molecular structure: bond length, r, in Å and angle, θ, in degrees.

ments for small molecules. Finally, a series of molecular dynamics calculations, starting from various configurations in which water molecules were placed in the membrane interior, was undertaken to directly observe dynamics of water molecules inside the membrane.

2. Methods

2.1. System and Force Field. We carried out a series of MD simulations of two bilayer systems, DPPC and DPhPC. Each bilayer system was composed of 72 lipid molecules hydrated by 2088 water molecules: The number of water molecules per lipid molecule was fixed at 29, which is almost the same as the experimental value (29.1) determined for the saturated DPPC bilayer.[13] The lipid molecules were modeled by the all-atom CHARMM force field (PARM27)[14] and the water molecules by modified rigid TIP3P water.[15] To build up the DPhPC model, all chiral *tert*-carbons were treated as having R configurations.[16] In our particle insertion calculations to evaluate the excess chemical potential, seven possible penetrants were used: H_2O, NH_3, O_2, CO, NO, CO_2, and $CHCl_3$. Force field parameters for these molecules were taken from the literature[14,17−20] and are listed in Table 1. All of these inserted molecules were treated as rigid bodies.

2.2. Molecular Dynamics Simulations (Equilibrated Bilayer Systems). Two molecular dynamics simulations were undertaken in the isothermal−isobaric ensemble.[21−23] The first simulation was carried out on the DPPC bilayer and the second was carried out on the DPhPC bilayer. The simulation time was 2.5 ns for each (the first 1 ns was for equilibration). The temperature of the system was set to 323 K, and pressure was tuned to 0.1 MPa. The Lennard-Jones interactions were truncated by applying a smooth switching function to the potential over the range of 10−12 Å.[24] The electrostatic interactions were calculated by the Ewald method.[26] Further simulation details were described elsewhere.[11] To check the equilibration of the system, we have monitored several structural and energetic quantities. The convergence of the cross-sectional area of a lipid molecule, which showed the slowest among those of all the monitored quantities, was used as a guideline for the equilibration. After equilibration, the averaged cross-sectional areas were 62.0 and 76.8 Å^2 for DPPC and DPhPC, respectively. The calculated peak-to-peak distances of the electron density profile (i.e., membrane thickness) were 39.6 and 38.2 Å in DPPC and DPhPC membranes, respectively. These calculated membrane dimensions were in good agreement with those obtained by experimental measurements.[13,25]

2.3. Free Energy Calculations. *A. Particle Insertion.* To estimate the free energy (FE) profiles of several small molecules along the bilayer normal, we used Widom's particle insertion technique with cavity-based sampling.[26] In the original Widom method, the excess chemical potential of a molecule is calculated by inserting it into a randomly selected position with a random orientation. The expression for the excess chemical potential in the NPT ensemble is

$$\mu_{ex} = -k_B T \ln\left\langle \beta \frac{P_{ext} V}{(N+1)} \exp[-\beta \Delta U] \right\rangle_N \quad (1)$$

where P_{ext} is the external pressure, V is the system volume, $\beta = 1/k_B T$, and ΔU is the interaction energy of the $(N+1)$th molecule with the all other molecules in the system. The brackets denote the NPT ensemble averaged over the configuration space of the particle and volume. For brevity, the expression for a one-component system is used here.

The Widom method is a powerful way to compute the chemical potential of a small molecule. The advantages of this method are its simplicity and low computational expense. It can be used just to analyze molecular configurations generated by the usual MD or MC simulations. However, the sampling efficiency of this method decreases as the size of the inserted molecule or the density of the system increases, because most trial insertions will not contribute appreciably to the average in eq 1.[26]

To overcome this disadvantage, several free-volume-based biasing procedures have been proposed.[12,27,28] The basic idea of these procedures is that selective trial insertions into the free volume in the system will increase the sampling efficiency of the Widom method. We used here a relatively simple method, the so-called "cavity insertion" Widom method,[12] to reduce the computational expense. In the cavity insertion method, we first select a free volume with a minimum radius R_{cav} and insert test molecules into that volume only. In this case, the free energy to form the cavity must be explicitly taken into account, and eq 1 should be written as

$$\mu_{ex} = -k_B T \ln\left\langle \beta \frac{PV}{(N+1)} \exp[-\beta \Delta U] \right\rangle_N - k_B T \ln\langle P_{cav} \rangle_N \quad (2)$$

where P_{cav} is the probability of finding a cavity with a radius of at least R_{cav}. To begin the cavity insertion method, the system is mapped to a uniform grid. If no atom lies in the grid, the grid is regarded as a cavity. The method significantly reduces computation time by considering neither the size distribution of the cavities nor the van der Waals radius of the system atoms. We applied this technique to the MD trajectories generated in the NPT ensemble.

The free energy profile of a single molecule along the bilayer normal, z, can be evaluated by the following relation:

$$\Delta G(z) = G(z) - G(z_0) = \mu_{ex}(z) - \mu_{ex}(z_0) \quad (3)$$

The reference state, z_0, can be arbitrarily selected; we chose the center of the water layer. The cavity insertion technique was used to estimate the free energy profiles of the seven molecules listed in Table 1. The simplicity of the cavity insertion technique allowed us to evaluate the excess free energy of multiple molecules at the same time without significant computational penalty. According to Jedlovszky and Mezei,[12] the

accuracy of the chemical potential estimation depends on the tunable parameter, R_{cav}. Therefore, we employed four different R_{cav} values, 2.6, 2.7, 2.8, and 2.9 Å, to check the convergence of the free energy estimation. For each R_{cav}, we undertook a series of cavity insertion calculations for which we shifted the grid position by half of the grid length in the *z*-axis; for example, at $R_{cav} = 2.6$ Å, we obtained the excess chemical potential at $z = 0$, 2.6, 5.2, ..., as well as $z = 1.3$, 3.9, 6.5,... We applied the cavity insertion to 30 000 configurations generated by NPT-MD. For each configuration, after dividing the system into a uniform grid, we selected 10 cavity grids at every *z* position. For each cavity selected, we carried out 10 trial insertions in randomly selected orientations of the test molecules. Thus, 3 million trial insertions were undertaken per slab to obtain the excess chemical potential. Since each insertion calculation can be performed independently, we used parallel computers to save time. The calculation of the free energy profile of the seven test molecules with one R_{cav} value took only about 23 h on a 10-node Compaq AlphaStation XP-1000 (21264 667MH) machine. During the cavity insertion sampling, the interaction between the penetrant and the system atoms was evaluated using a cutoff at the length of 20 Å instead of the Ewald sum. The error due to the truncation of the interaction was much smaller than was the statistical error.

B. Probability Ratio Method. The free energy profile of a water molecule across a membrane can also be estimated by the local equilibrium water concentration along the bilayer normal.[29]

$$\Delta G(z) = G(z) - G(z_0) = -k_B T \ln \frac{\int d\mathbf{h} \int d\mathbf{r} \delta(r_{w,z} - z) \exp[-\beta(U + P_{ext}V)]}{\int d\mathbf{h} \int d\mathbf{r} \delta(r_{w,z} - z_0) \exp[-\beta(U + P_{ext}V)]} = -k_B T \ln \frac{P(z)}{P(z_0)} \quad (4)$$

where r_w is the configuration of water molecules and $P(z)$ is the probability density of the water at *z*. This relation enables us to obtain the free energy profile of a water molecule by analyzing the local densities of the MD trajectories. The bilayer system was sectioned into slabs along the bilayer normal, and the water density in each slab was averaged over the time-course of MD calculations. During the MD runs, however, we observed no water penetrating into the hydrophobic region of the bilayer beyond the carbonyl carbon.[11] According to eq 4, this allowed us to deduce an inaccurate picture in which the bilayer contains an infinite energy barrier against water. This misleading result is clearly attributable to the limited simulation time (and space); it would be very unlikely to observe water migrating into the bilayer interior during the usual MD time (~ns). While the probability ratio method does not work in a region that has a low water concentration, it does provide a well-converged free energy profile of water in the region from the bulk water to the interface, where the cavity insertion technique shows some loss of accuracy.

C. Thermodynamic Integration. It is possible to use thermodynamic integration (TI)[26] to estimate the free energy profile of a molecule across a membrane.[29] In this application, the thermodynamic integration path is along the bilayer normal, *z*, and the free energy difference between the two states of a penetrant (e.g., inside and outside the membrane) is written as

$$\Delta G^s(z) = G^s(z) - G^s(z_0) = \int_{z_0}^{z} \left(\frac{\partial G}{\partial r_{s,z}} \right) dr_{s,z} = \int_{z_0}^{z} \left\{ \frac{\int d\mathbf{r}^N d\mathbf{h} \left(\frac{\partial U}{\partial r_{s,z}} \right) \exp[-\beta(U + P_{ext}V)]}{\int d\mathbf{r}^N d\mathbf{h} \exp[-\beta(U + P_{ext}V)]} \right\} dr_{s,z} = \int_{z_0}^{z} \left\langle \frac{\partial U}{\partial r_{s,z}} \right\rangle_{rs,z} dr_{s,z} = -\int_{z_0}^{z} \langle F_{s,z} \rangle_{rs,z} \, dr_{s,z} \quad (5)$$

where $\langle \rangle_{rs,z}$ denotes an ensemble average for a system in which the *z*-coordinate of the center of mass (COM) of the penetrant is fixed at $r_{s,z}$.

We used the TI method to estimate the free energy of a water molecule. To obtain a free energy profile across a membrane, we used a series of constrained MD simulations[30] to measure the average force exerted on the water molecule fixed at a given depth $r_{s,z}$ in the membrane, and then integrated the force along the *z*-axis across the membrane. During the constrained MD, only the *z*-coordinate of the inserted water COM was fixed; the water could diffuse along the $x-y$ plane and rotate freely. A precise estimation of the average force can be obtained only by a lengthy MD simulation. For example, the free energy gradient obtained by TI, which was based on the average force calculation estimated by 100 ps MD at each fixed point, showed a significant dependence on the permeation path, i.e., the local environment for the constrained water.[31] Thus, lengthy constrained MD calculations are necessary for each fixed point. For greater effectiveness, when TI is employed to estimate the free energy profile of a water molecule across the membrane, the average force calculation should be undertaken along dozens of possible permeation paths. In any case, TI demands quite a long computation time, though it can potentially yield accurate free energy estimations when the sampling number is increased. In this study, we carried out a series of 100 ps constrained MD simulations in which a water COM was fixed only at distances of 0, 3, 6, 9, and 12 Å from the bilayer center. The constrained MD calculation was conducted 10−20 times at each fixed point, with different starting configurations. Since a 3 Å mesh would be too rough to obtain a free energy profile thoroughly by the TI calculation, we used the average force only as a correction of the free energy profiles measured by the cavity insertion and probability ratio methods. The main reason extensive constrained MD calculations were undertaken here was to evaluate the local diffusion coefficients of water molecules inside the membrane. That method is described in the next section.

2.4. Local Diffusion Coefficients. The "local" diffusion coefficient of a water molecule is used not only to characterize the position dependent mobility or local friction along the bilayer normal but also to estimate the permeation rate by the equation (see eq 9 in section 3.2) proposed by Marrink and Berendsen.[29] We used two different methods to estimate the local diffusion coefficient of a water molecule along the bilayer normal. The first method was based on the mean-square displacement (MSD),[32] and the second was an estimation by the force autocorrelation function (FACF).[29,33]

The slope of the MSD curve is proportional to the diffusion coefficient,

$$D(z) = \frac{1}{2d} \lim_{t \to \infty} \frac{1}{t} \langle |\mathbf{r}(t) - \mathbf{r}(0)|^2 \rangle_z \quad (6)$$

where d denotes the dimension. MSD sampling was carried out for the water found in $z = z \pm \Delta z$ at $t = 0$, and Δz was taken to be 1.5 Å in our calculations. Since the water molecules leave the home slab at a large t, we cannot estimate net "local" diffusion coefficients using the slope at t being infinity. (In such a sampling, diffusion coefficient is not a function of z anymore.) Therefore, the "local" diffusion coefficient was estimated using short-time (2−6 ps) MSD slopes instead. Although the choice of the time range for the MSD fitting is not unique, we found a linear MSD slope in this time range, and the calculated D was not so sensitive to the fitting range: even if we extended the time range to 2−10 ps, the calculated D was almost within the statistical error. (Note that, in the middle of the water layer, water molecules migrate out of the home slab rather rapidly, i.e., within several ps,[34] and the obtained diffusion coefficient became slightly smaller with elongating the time range for the fitting beyond 10 ps.) Whenever a water molecule was found in the slab, the local diffusion coefficient of a water molecule along the bilayer normal, D_z, as well as that in the bilayer plane, D_{xy}, were evaluated separately using this method.

The FACF method is an alternative way to estimate the local diffusion coefficients of water molecules.[29] In this method, the local diffusion coefficient is evaluated by the following relation:

$$D(z) = \frac{(RT)^2}{\int_0^\infty \langle \Delta F_{s,z}(t) \Delta F_{s,z}(0) \rangle \, dt} \tag{7}$$

where R is the gas constant and $\Delta F_{s,z}(t) = F_{s,z}(t) - \langle F_{s,z} \rangle$ is the deviation of the instantaneous force exerted on the water molecule fixed at $z = z$. As in the TI method, a series of constrained MD simulations is needed to estimate the local diffusion coefficient with good accuracy, because FACF will, like TI, show path-dependency. The merit of the FACF method is that it can estimate local diffusion coefficients at positions where water molecules are seldom found because of a high free energy barrier (i.e., inside the bilayer membrane), whereas a constrained MD simulation of the entire bilayer system is needed in order to obtain only one component: the force exerted on the fixed water molecule.

2.5. Molecular Dynamics Simulations (Relaxation from a Nonequilibrium Configuration). To observe the water dynamics in the hydrocarbon region of each bilayer directly, a series of MD simulations, starting from various configurations of four water molecules located inside the bilayer, was undertaken in the canonical ensemble. The starting configurations were basically taken from those produced during the NPT-MD simulation, after which four selected water molecules were picked and placed at the bilayer center. The distance between molecules in any given pair of the inserted water molecules was taken to be larger than 20 Å; each inserted water molecule was isolated in a hydrophobic environment initially. The reasons to take four water molecules inside membrane initially are not only to obtain more statistics for dynamics of the water molecule from the limited number of MD runs but also to examine whether the clustering of these water molecules occurs or not in the hydrophobic bilayer interior. After the energy of these four water molecules was minimized, a short time, say 1 ps, an equilibration NVT-MD run was carried out. Then, another 200 ps NVT-MD simulation was undertaken. The above set of calculations was conducted a total of 10 times for the DPPC and DPhPC bilayer systems, respectively. Similarly, several MD simulations were conducted for both systems, starting from initial configurations where a single water molecule was inserted in the vicinity of the bilayer center until the inserted water escaped from the membrane interior.

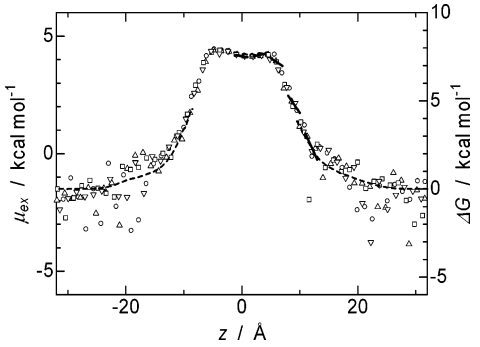

Figure 1. The excess chemical potential (free energy) profile of water molecules along the bilayer normal in the DPPC bilayer. The four dots (open circle: $R_{cav} = 2.6$ Å, open triangle: $R_{cav} = 2.7$ Å, open square: $R_{cav} = 2.8$ Å, and open inverse triangle: $R_{cav} = 2.9$ Å) are the excess chemical potentials obtained by the cavity insertion technique. The dotted line is the free energy profile measured by the probability ratio method. The thick solid lines are the free energy gradients estimated by thermodynamic integration (average force). The origin of the abscissa was taken to be the bilayer center.

3. Results and discussion

3.1. Free Energy Profile. Figure 1 shows the excess chemical potential profile of water as a function of the position along the DPPC bilayer normal. The figure plots the excess chemical potential estimated by the cavity insertion technique with each of four minimum radii, $R_{cav} = 2.6$, 2.7, 2.8, and 2.9 Å. The convergence of the chemical potential was fairly good in the hydrophobic region of the bilayer, $|z| < \sim 15$ Å. In the interfacial region, however, the excess chemical potential is estimated at a lower resolution because of relatively high density of the system atoms in the region. The excess chemical potential profile in Figure 1 reveals that a free energy barrier of ∼6.3 kcal/mol exists for water across the DPPC bilayer. The barrier height and the profile, including a shallow trough at the center of the bilayer, are comparable to those obtained by the previous free energy calculation on the basis of MD simulation,[29] in which a modified united-atom GROMOS force field[35] and the SPC water model[36] were used to build the DPPC bilayer system. A recent extensive TI study of the dimyristoylphosphatidylcholine (DMPC) bilayer using the united-atom OPLS force field and the TIP4P water model provided a similar free energy barrier.[31] However, another free energy study used the cavity insertion Widom method and found a significantly high free energy barrier, about 13.5 kcal/mol, for a water molecule across the DMPC membrane.[12] In that study, cavity insertion was performed on only 1500 configurations generated by NVT-Monte Carlo of a small bilayer system using the all-atom CHARMM22 force field. Therefore, we consider the present simulation is statistically more reliable compared with the MC calculation.

The excess chemical potential profiles obtained by the four different R_{cav} were quite similar to each other, though the variance was large near the interface. This indicates that the free energy profile calculated by cavity insertion is not so sensitive to the choice of R_{cav} value in the range used here. The R_{cav} dependence of the calculated chemical potential was checked by a series of cavity insertion calculations on a pure TIP3P water system. The details appear in the Appendix.

Figure 1 also shows the free energy profile of water obtained by the probability ratio method as well as the free energy gradient estimated by TI calculation. The curves well fit those

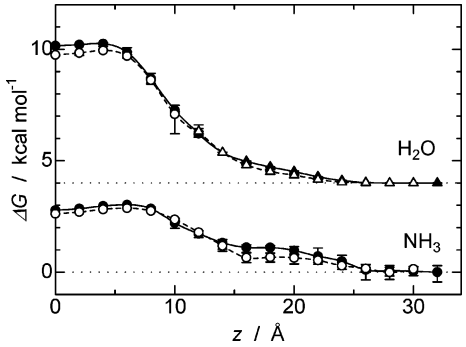

Figure 2. Free energy profiles of water and ammonia as a function of the distance from the bilayer center. The closed symbols denote the free energy profiles across the DPPC bilayer. The open symbols denote those across the DPhPC bilayer. The circles and triangles are the free energy estimated by the cavity insertion and that estimated by the probability ratio method, respectively (the latter for the case of water only). For clarity, the water data are shifted by 4 kcal/mol.

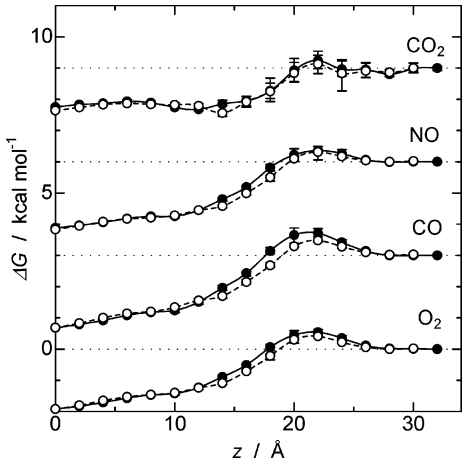

Figure 3. Free energy profiles of O_2, CO, NO, and CO_2 across the membrane. Closed circles and open circles represent the free energy profiles across the DPPC bilayer and those across the DPhPC bilayer, respectively. For clarity, the data of CO, NO, and CO_2 are shifted by 3, 6, and 9 kcal/mol, respectively.

obtained by cavity insertion. The probability ratio method provides a well-converged free energy profile from the bulk water layer to the interface ($|z| \geq 12$). Thus, a combination of the probability ratio method and cavity insertion will be a way to yield a well-converged free energy profile of a water molecule with minimal computational cost. The agreement among the free energy profiles calculated by these different techniques convinced us that the calculated free energy profile is correct to within a small statistical error.

Figures 2−4 show the free energy profiles of seven small molecules across DPPC bilayer and across DPhPC bilayer. In these plots, assuming the symmetric structures of the bilayers, the free energy values were averaged between the two sides of the bilayer and the profiles across half of the membrane are plotted. To obtain a smooth free energy profile, a Gaussian filter was applied to the excess chemical potential as

$$\mu'(z_i) = \frac{\sum_j^{N_{\mathrm{data}}} \exp(-(z_j - z_i)^2/\sigma^2)\cdot\mu(z_j)}{\sum_j^{N_{\mathrm{data}}} \exp(-(z_j - z_i)^2/\sigma^2)} \qquad (8)$$

where $N_{\mathrm{data}}(= 190)$ is the number of original $\mu(z_j)$ data, each of

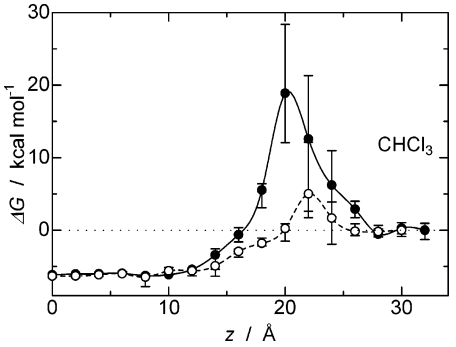

Figure 4. Free energy profile of $CHCl_3$ across the membrane. The symbols are the same as in Figure 3.

which was estimated by >3 million trial insertions. The variance parameter, σ, used in our calculation was 1 Å, which effectively removed the statistical noise without significantly changing the profile. The error bars shown in these figures denote the variance of the original μ values from the filtered profile. In the case of water only, the free energy profile is given by a combination of the cavity insertion method ($|z| \leq 12$ Å) and the probability ratio method ($|z| \geq 12$ Å).

The obtained free energy profiles of water shown in Figure 2 reveal that the two bilayers give rise to quite similar free energy barriers. A slight difference between these two profiles is the barrier height: ∼6.3 and ∼6.0 kcal/mol for DPPC and DPhPC bilayers, respectively. As described above, the convergence of the excess chemical potential in the middle part of the membrane is fairly good, with an estimated error of ∼0.1 kcal/mol. Thus, assuming the same excess chemical potential of a water molecule in the bulk water region, the branched DPhPC bilayer can have a slightly smaller energy barrier for a water molecule, although the difference was much less than *kT*. (This assumption may be reasonable, because the free energy curve calculated from the local density difference showed that there was no free energy gradient in the bulk water region ($|z| >$ ∼27 Å), and nearly identical hydration structures were observed at the interface of the two lipid bilayers.[11]) These findings are consistent with the previous experimental observation that chain branching does not change the solubility of water into the hydrocarbon liquids (*n*-hexadecane: 95.5 g/cm^3 and 2,6,10,15,19,23-hexamethyl tetracosane: 102.0 g/cm^3 at 318 K).[10] At the bilayer center, a small depression of about 0.2 kcal/mol in the excess free energy profile was observed in both systems. The low local density of the system atoms in the vicinity of the slip plane between two leaflets of the bilayers would cause the small depression. A similar hollow is observed commonly in the free energy profiles of small molecules.

Figure 2 also plots the free energy profile obtained for ammonia. The shape of the curve was similar to that obtained for water, though the resolution of the free energy was low in the interfacial region. Comparison between the lipid bilayer systems revealed only a small difference, with barrier heights of ∼3.0 and ∼2.9 kcal/mol in DPPC and DPhPC bilayers, respectively. These barrier heights were about half those obtained for water. The barrier was lower because molecular dipole moment of ammonia is smaller than that of water (μ_{H_2O} = 2.45 D and μ_{NH_3} = 1.47 D); the loss of electrostatic free energy is relatively small when an ammonia molecule, instead of a water molecule, moves from the bulk water region to the bilayer center.

The free energy profiles of three diatomic molecules, O_2, CO, and NO, were quite similar to each other (Figure 3) and were completely different from those of water or ammonia. O_2 is a

nonpolar molecule, and the dipole moments of the other two were very small (<0.2 D). Thus, these three molecules preferred the hydrophobic environment and were energetically stabilized inside the bilayer membrane. The variation in free energy profiles due to lipid chain branching was negligible. In addition to the cases of water and ammonia, these three molecules also exhibit a small trough in the free energy profile in the middle of the bilayer due to low local density of the system atoms there. The free energy advantages by translocating O_2, CO, and NO from bulk water to the center of the bilayer were calculated to be 1.9, 2.3, and 2.1 kcal/mol, respectively, in each bilayer system. A tiny free energy barrier appeared in the interfacial region, though it was not observed in the previous studies.[12,17] For these three small molecules, the calculated excess chemical potential converged well, and the error among four different R_{cav} values was less than ~0.2 kcal/mol, even in the interfacial region. The barrier heights are slightly larger than the error. Thus, we consider that the possible small free energy barrier could stem from the ordered interfacial structure. In Figure 3, the free energy profiles of CO_2 are also plotted. Again, no difference was identified between the free energy profile across DPPC bilayer and that across DPhPC bilayer. Since it is a nonpolar molecule, CO_2 also gains a small amount of free energy, about 1.3 kcal/mol, by moving into the bilayer. The flat profile indicates that CO_2 (also other nonpolar molecules: O_2, CO, and NO) can pass through the membrane with little activation energy. The variation of the free energy barrier of these penetrants across the bilayers is, in general, consistent with the change of the permeation rate experimentally observed for lipid membranes.[37−39]

The free energy profiles of $CHCl_3$ show quite different behavior from the other test molecules. A large peak was observed in the free energy profile across DPPC bilayer, as was observed in the previous cavity insertion study on DMPC bilayer. Furthermore, the existence of the free energy barrier near the interface was also predicted by an additional TI calculation.[12] In the free energy profile across DPhPC bilayer, however, we measured only a much smaller peak. Because $CHCl_3$ molecules are large, the resolution of the free energy of $CHCl_3$ is relatively low in the interfacial region. Nevertheless, the qualitative difference between DPPC and DPhPC membranes may have various implications. One clear difference in the interfacial region is the molar fraction of water. As previously described in our paper,[11] the larger molecular area of DPhPC relative to that of DPPC allows more water to reside in the interfacial region. The change in the local molecular fraction might provide the necessary difference in the environment to support a large and polar (μ_{CHCl_3} = 1.07 D) $CHCl_3$ molecule. It is noteworthy that, apart from the difference near the interface, the solubility of $CHCl_3$ into the hydrophobic membrane core is identical between these two bilayer systems.

3.2. Water Dynamics. Although lipid chain branching does not significantly alter the free energy profile of the water molecule, the branched chain's slower conformational motion, which was observed in our preceding paper,[11] suggests that the dynamics of water (or of any penetrant) in the membrane interior will be changed significantly. Figure 5 plots the local diffusion coefficients of water molecules along the bilayer normal, D_z, as a function of the distance from the bilayer center.[40] These coefficients were calculated by means of MSD ($|z| \geq 12$ Å) and FACF ($|z| \leq 12$ Å). At $|z| = 12$ Å, the D_z values estimated by these two methods showed a subtle discrepancy. MSD yields a larger $D_z(z)$ in both bilayer systems. Although the MSD calculation was applied to the water molecules located in the slab (width 3 Å), the local density was not uniform in the interfacial region and was always larger in the outer membrane. In addition, most water molecules diffuse toward the outside of the membrane near the interface. Thus, MSD tends to overestimate diffusion coefficients in the interfacial region. On the other hand, the accurate estimation of D_z using FACF is not easy statistically, because a large-scale constrained MD simulation has to be undertaken to yield only one component of the force exerted on the constrained water. Though we have carried out constrained MD runs of more than 15 ns to estimate local diffusion coefficients at only 10 points (5 points for each bilayer system), the calculated D_z still contains rather large statistical noise. (Note that the error bars for FACF-based D_z shown in the figure denote just the error arising from the integration of FACF.) We adopted two criteria for checking the convergence of FACF-based D_z. (1) The calculated D_z agrees with the one estimated by MSD at $|z| = 12$ Å. (2) Potential of mean force (i.e., average force: gradient of the free energy profile along the bilayer normal, see eq 5) converged to the value that is consistent with the free energy profile obtained by both the cavity insertion and probability ratio methods as shown in Figure 1. The calculated data satisfy these criteria, and the qualitative difference between these two bilayers is quite evident. Therefore, we believe that it is meaningful to compare the mobility of water inside DPPC and DPhPC bilayers.

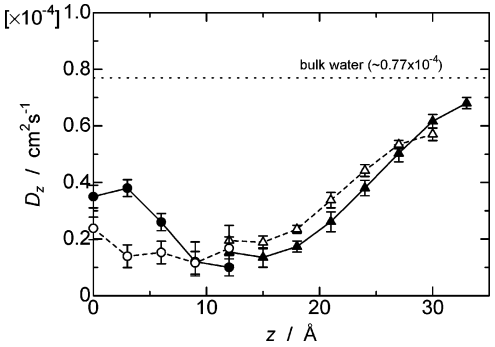

Figure 5. Local diffusion coefficients of a water molecule in the normal direction of the bilayer, D_z, as a function of the distance from the bilayer center. The circles and triangles are the D_z values determined using the force autocorrelation function and mean square displacement, respectively. The closed and open symbols are D_z in the DPPC and DPhPC bilayers, respectively.

The local diffusion coefficient profile of water in DPPC bilayer revealed the following. (1) The diffusion coefficient in the middle of the water layer is comparable to that observed in pure TIP3P water (~0.77×10^{-4} cm^2/s at 323 K; note that modified TIP3P water used here overestimates the experimental diffusion coefficient by a factor of ~2). If we construct the system with larger concentration of water, it will be expected that the diffusion coefficient in the water layer completely coincides with that of bulk water. Although the slightly smaller diffusion coefficient observed in the middle of the water layer is, in this sense, a finite size effect of the simulated system, it should be noted that, in our simulations, the hydration level is fixed at 29 water/lipid, which is consistent with the saturated hydration for DPPC bilayer.[13] (2) From the bulk water to the interfacial region, $|z| > 15$ Å, the local diffusion coefficient of water decreases monotonically as water molecules near the interfacial region. (3) The translational mobility of the water located in the region of $|z| = 9-15$ Å is significantly low. (4) In the hydrophobic region of the bilayer, $|z| < 9$ Å, water diffusion was promoted in the vicinity of the slip plane between the two leaflets of the bilayer.

It should be noted here that the calculated diffusion coefficient of water in the bilayer interior is much smaller than that of bulk water. In a previous report,[29] the diffusion of water was significantly enhanced in the bilayer interior; the rate was estimated to be about twice that of bulk water. The discrepancy would stem partly from the different potential models: all-atom representation for the alkyl chains in the present study and united-atom representation in the previous study. A comparison of the diffusion coefficient profiles between DPPC and DPhPC bilayers demonstrates that chain branching reduces water diffusion significantly in the hydrophobic membrane interior. In the DPhPC bilayer, although diffusion was still found to be enhanced in the vicinity of the slip plane, the low diffusion coefficient almost plateaus in the range of $|z| = \sim 3-9$ Å, demonstrating that the mobility of water is significantly affected by the slow conformational motion of the branched chain.[11] In the interfacial region, on the other hand, the water diffusion is relatively fast in DPhPC bilayer. This enhanced diffusion can be explained by the higher exchange rate of the phosphate-bound water,[11] which would be partly due to the larger molecular area of DPhPC.

The local diffusion coefficients in the bilayer plane, D_{xy}, were also calculated for both bilayers. The profiles are given in Figure 6. In the region of $|z| \leq 12$ Å, the $D_{xy}(z')$ values were calculated by the MSD of the water constrained in the bilayer plane, $z = z'$. The restrained water showed slightly smaller D_{xy} at $|z| = 12$ Å than the unrestrained water. The profiles of D_{xy} are qualitatively similar to those of D_z. In the lipid bilayer, lateral water diffusion is severely restricted in the range of $|z| = 10-15$ Å. As a result of chain branching, a water molecule diffuses more slowly in the membrane interior and more rapidly in the other regions. Thus, lipid chain branching significantly reduces both the lateral and normal diffusion rates of water in the bilayer interior. A comparison between D_{xy} and D_z reveals that the water favors lateral diffusion except at the interfacial region, $|z| = 9-20$ Å. In the interfacial region, however, lateral diffusion of the water molecule is significantly suppressed. This brings to mind an image in which the dynamics of the water molecule in the interfacial region is restricted to a narrow path formed by the surrounding segments of the lipid molecules. Once the water reaches the hydrophobic membrane interior, however, it has several paths or a large free space stretched along the bilayer plane.

Once the free energy and local diffusion coefficient profiles of water across the membrane are obtained, it is possible to estimate the permeability coefficient, P, using the following relation:[29]

$$1/P = \int_{z_1}^{z_2} \varsigma(z)\, dz = \int_{z_1}^{z_2} \frac{\exp(\Delta G(z)/kT)}{D_z(z)}\, dz \qquad (9)$$

The integrand of the above equation, $\varsigma(z)$, denotes the local resistance to the permeation at z. Taking $z_1 = -30$ and $z_2 = 30$ Å, the permeability coefficients of water across DPPC and DPhPC bilayers were estimated to be about 1.6×10^{-2}cm/s and 1.1×10^{-2}cm/s, respectively. As described above, since components in the integrand of eq 9 themselves showed large statistical errors, the calculated permeability also contained a large degree of error. In addition, the experimentally determined permeability showed wide variation, from 10^{-2} to 10^{-4},[2,4,41-45] because the values are sensitive to the experimental techniques and conditions, such as bilayer systems (liposomes or planar lipid bilayers), salt concentration, and pH. Therefore, we restrict our discussion to the qualitative difference in the permeability of DPPC and DPhPC bilayers. In our calculations, chain branching reduces the permeability of water only by about 30%. Similarly, a comparative measurement of water permeability across DPhPC ($4.29 \pm 0.30 \times 10^{-3}$cm/s) and across straight-chained *E. coli* lipid bilayers ($4.9 \pm 0.16 \times 10^{-3}$cm/s) suggested that the presence of branching methyl groups did not have a major effect on water permeability.

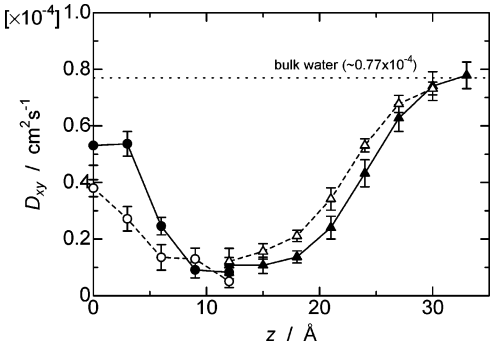

Figure 6. Local diffusion coefficients in the bilayer plane, D_{xy}, as a function of the distance from the bilayer center. The circles and triangles are the D_{xy} values determined using mean square displacement (MSD) of the water constrained in a bilayer plane and those determined using MSD of the free water, respectively. The closed and open symbols are D_{xy} in DPPC and DPhPC bilayers, respectively.

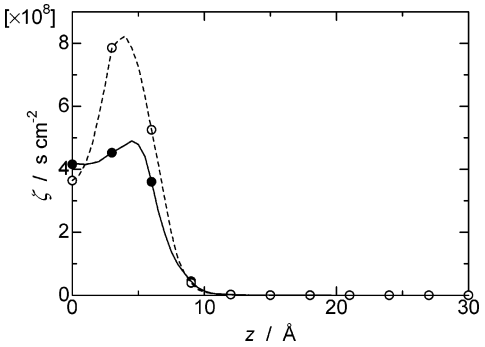

Figure 7. Permeation resistance of a water molecule as a function of the distance from the bilayer center. Closed circles and solid line: the profile across DPPC bilayer. Open circles and dashed line: the profile across DPhPC bilayer. The lines are drawn by the data every 0.5 Å calculated by interpolations of the free energy and local diffusion coefficient profiles.

Figure 7 plots the local resistance to permeation as a function of the distance from the bilayer center. Both lipid bilayers show their highest resistance to water permeation around $|z| = 4-5$ Å (i.e., in the middle of the hydrophobic chain), although the resistance is much greater in the DPhPC bilayer than in the DPPC bilayer in that region. On the other hand, local resistance differs only slightly in the vicinity of the center of the bilayer. The depression of the resistance at the bilayer center should be related to the low density of the system atoms occurring from a slip plane between the two leaflets of each bilayer. In our preceding paper,[11] a comparison of the trans-gauche isomerization rate in the hydrophobic chain demonstrated that the branched chain had a much lower rate than its straight counterpart in the middle of the chains, whereas only a small rate reduction resulted from chain branching in the tail region (from C12 to C15). This revealed that the difference in the permeation resistance to water correlates significantly with the difference in the mobility of the lipid chains. In other words, the lipid conformation more or less limits the water dynamics, at least in the hydrophobic membrane interior.

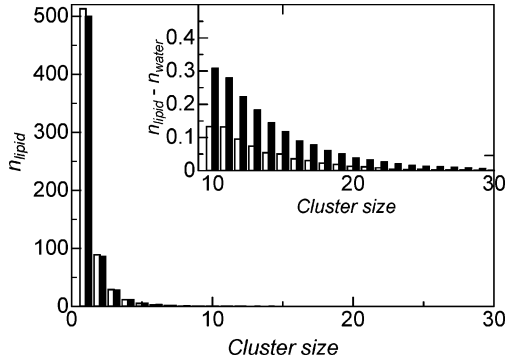

Figure 8. Distribution of cavity clusters according to size. Solid bars: DPPC. Open bars: DPhPC.

3.3. Cavity Distribution. As we mentioned in the case of water, the dynamics of many small penetrants are significantly affected by the lipid chain conformation in the membrane interior, because the relaxation time of chain conformation is usually much longer than the characteristic time of translational motion of small penetrants. In this sense, the analysis of the cavity distribution in the lipid bilayer system will shed light on the dynamical behavior of the small (at least, neutral) molecules in the membrane interior. For the analysis of cavity distribution in the bilayers, we first mapped each system to a uniform grid. The grid size was taken to be 2.9 Å here. If no system atom lay in a grid point, the grid was denoted as a cavity. For simplicity, we did not take the van der Waals radii of the atoms into account. This approximation did not change the qualitative and statistical discussion with respect to the difference between the straight and the branched chains.

First we analyzed the size distribution of cavities on a cubic $22 \times 22 \times 22$ lattice in each bilayer. If two neighboring grid points were labeled as cavities, they were regarded as members of the same cluster. Figure 8 presents the distributions of cavities according to their sizes in the bilayer systems, averaged over the length of MD. These distributions revealed that it was most probable for a cavity to be isolated, showing an exponential decay of the probability as a function of cluster size, although the large clusters of cavities did exist in both DPPC and DPhPC bilayer systems. To clarify the cavity distribution inside the lipid bilayers, the same analysis was done on a pure water system, and the number of cavity clusters in the pure water, n_{water}, was subtracted from that in the lipid bilayer, n_{lipid}, so that the distribution of ($n_{lipid} - n_{water}$) could be plotted (see inset of Figure 8). The results showed that large cavities were probably formed in the bilayer region and that the DPPC bilayer has a higher probability of large cavities than the DPhPC bilayer does.

Thus, lipid chain branching prevents a large free volume from forming in the hydrocarbon region of the bilayer. Because the cavity clusters measured here are larger than the dimensions of a methyl group, it is reasonable to suppose that the discrete, smaller size distribution of free volume in DPhPC bilayer may be caused not only by the hindrance of methyl group but also by conformational change of the chain. This is evidenced by the branched chains bending selectively at the branching carbons (*tert*-carbons) and by the frequently observed chain "entrapment" between the lateral neighboring lipids in DPhPC bilayer.[11]

Although the above analysis was conducted on instantaneous configurations of these two bilayer systems, from the standpoint of the permeation process of small (neutral) molecules, analysis should take into account the lifetime and geometrical distributions of free volume pockets in lipid bilayers. In this sense, time-averaged cavity distribution is worthy of analysis. The

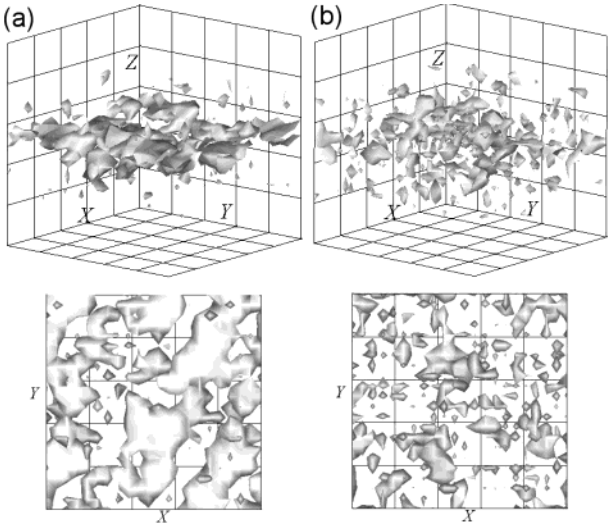

Figure 9. Cavity distribution in the lipid bilayers averaged over 1.5 ns MD trajectories. The isosurface shows the probability of cavity formation at a level of 0.15. (a) DPPC and (b) DPhPC bilayer systems. The bottom of each is the view from the bilayer normal, *z*. As a guide for the eye, the grid is drawn at regular intervals of 12.2 Å.

cavity probability of the uniform grid was averaged over 1.5 ns MD trajectories. The isosurface at the level of $P = 0.15$ is drawn in Figure 9. In the figures, the *z*-axis is parallel to the bilayer normal and the bilayer center is located in the middle of the cubic box. The isosurface appears only inside the hydrophobic region of the lipid bilayers. The cavity probability in the water region ($P \sim 0.10$) and that in the interfacial region ($P \sim 0.05$) were significantly lower than the isolevel shown in the figure. The smaller size and high mobility of the water molecule reduce the time-averaged probability of cavity formation in the water region, and the high density of the system atoms at the water/lipid interface explains the lower cavity formation probability in the interfacial region.

Both DPPC and DPhPC bilayers presented high probabilities of cavity formation near the slip plane between two leaflets of each bilayer. However, the three-dimensional cavity distributions in these bilayers differed significantly from each other. In the DPPC bilayer system, the larger cavity domains were observed near the slip plane. In contrast, the DPhPC bilayer demonstrated discrete distribution of small cavities throughout the hydrophobic membrane domain. Although the appearance of the isosurface depends on the averaging time, the qualitative discussion should be meaningful when we consider the environment for penetrants in a hydrophobic membrane interior.

The difference in cavity distribution suggested that chain branching causes the following changes in the behavior of small penetrants inside the membranes: (1) The mobility of penetrants in the membrane interior will become low. (2) The probability of penetrants clustering in the membrane interior will become low. In light of cavity distribution revealed here, let us now discuss the dynamical behavior of small penetrants in the membrane interior, assuming that the dynamics of the penetrants is limited by the cavity distribution in the membrane. Since the discrete distribution of small cavities in a hydrophobic membrane interior would limit the motion of penetrants, the penetrants would be expected to show a restricted, hopping-like motion among the long-lived cavities. The restriction of penetrant motion should be remarkable in the branched DPhPC bilayer. In the DPPC bilayer, the distribution of high cavity-formation probability was spread along the lateral direction near the slip plane, which suggested that penetrants would likely

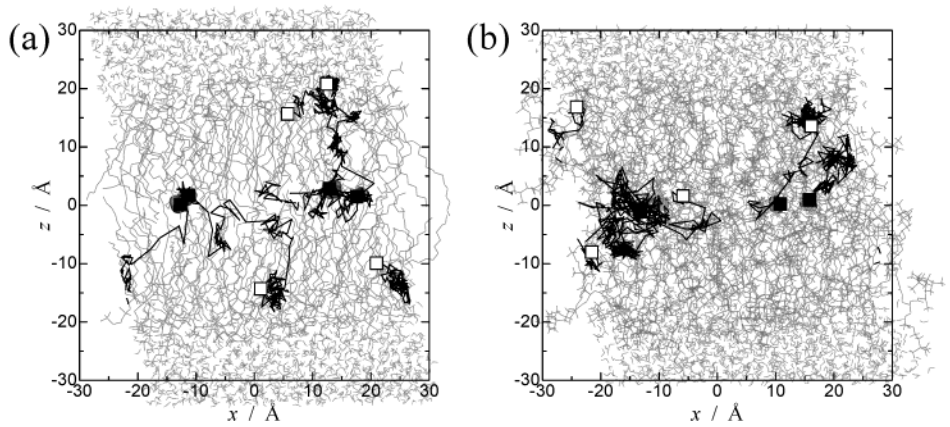

Figure 10. Typical trajectories of the four water molecules disposed near the bilayer center initially in (a) DPPC and (b) DPhPC bilayers. Initial and final (200 ps later) coordinates of the water centers of mass are plotted as closed and open squares, respectively.

migrate along the plane. It is expected that, during the lateral diffusion, the penetrants find a possible normal pathway to escape from the membrane region. On the other hand, in the DPhPC bilayer, even lateral diffusion of a penetrant will be relatively limited. This is consistent with our observation of local diffusion coefficients of water.

Temporal proton-wire (a transient hydrogen bonded chain of water molecules) formation through the lipid bilayer may be one of the most plausible explanations of abnormally high proton permeability.[2,44,46−48] In that hypothesis, the proton is transferred through the hydrogen bond network that the proton wire has formed. On the basis of the proton-wire hypothesis, let us consider the difference in proton conductance between straight-chained egg yolk PC ($17 \pm 3 \times 10^{-4}$ cm/s) and DPhPC ($3.6 \pm 1.1 \times 10^{-4}$ cm/s) bilayers[8] in light of the reduction of water mobility in the hydrophobic region as a result of lipid chain branching. At the slip plane (bilayer center) there exists a shallow free energy well due to the low density. Therefore, once a small penetrant goes into the region, it will stay there for a while and diffuse along the plane. According to Marrink and Berendsen, water trapped in the center of a bilayer had a lifetime of more than several tens of picoseconds.[29] We performed several trial MD runs from the initial configuration, where a water molecule was placed near the slip plane. From these trials, we observed that the lifetime of a single water molecule in the hydrophobic region was typically about ∼100 ps, and eventually, in the DPhPC bilayer, it reached over several hundred picoseconds. During the residence time, once a water molecule meets other water inside the bilayer, these water molecules will gain electrostatic stabilization. The clustering of the water molecules in the hydrophobic membrane interior may trigger the formation of a proton wire. This suggests that the relatively discrete distribution of small cavities in the DPhPC bilayer reduces the proton conductance significantly. On the other hand, as shown above, the presence of branching methyl groups did not have a major effect on water permeability. Thus, we consider that the inhibited clustering of water molecules inside the membrane may be responsible for the behavioral difference between proton and water permeability resulting from chain branching.

3.4. Molecular Dynamics Simulations (Relaxation from a Nonequilibrium Configuration). To obtain supporting evidence for the above view of the water dynamics in the membrane interior, we undertook a series of 200 ps NVT-MD calculations, starting from various configurations in which four water molecules were placed near the membrane center. The detailed condition of these calculations is described in section 2.5. Figure 10 presents typical examples of trajectories of the inserted water

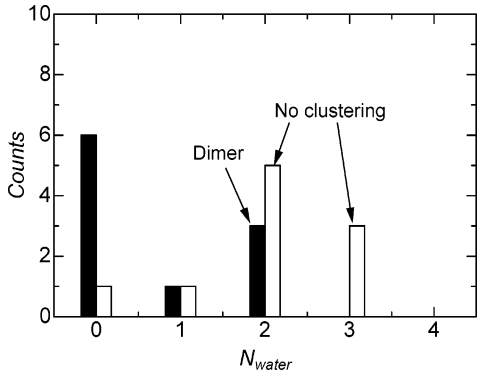

Figure 11. Histogram showing the distribution function of the number of water molecules remaining in the membrane interior after 200 ps, N_w (from a total of 10 MD trial runs for each bilayer system). Solid bar: DPPC bilayer. Open bar: DPhPC bilayer.

molecules in DPPC and DPhPC bilayers. The results demonstrated that water molecules in DPPC bilayer migrated rapidly near the slip plane at first; then, after escaping from the shallow free energy well at the bilayer center, the water showed restricted librational motion in the region of $|z| \sim 9-18$ Å and gradually moved to the bulk water region. On the other hand, water molecules in the DPhPC bilayer seemed to be entrapped in a small space in the hydrophobic region for a long time, and their migration was significantly restricted in any direction. The difference in water behavior was evident in the range of $|z| <$ 10 Å. The number of water molecules remaining in the membrane interior after 200 ps, N_w, was counted in 10 trial MD runs. The distribution function of N_w is illustrated in Figure 11. During the counting, any water molecule involved in a hydrogen-bond network formed by the bulk water was regarded as having escaped from the membrane. In almost all cases of DPPC bilayer, no water remained in the membrane interior after 200 ps, although we obtained three final configurations in which two water molecules still remained in the vicinity of the bilayer center as a dimer. Rapid lateral migration in the DPPC bilayer makes it possible for the water to meet the other inserted water. The electrostatic stabilization that results from cluster formation accounts for the longer residence time of the dimer in the hydrophobic environment. In contrast, in the DPhPC bilayer, two or three isolated water molecules usually remained in the membrane interior even after 200 ps. Each of the remaining water molecules seemed to be entrapped in a small cavity formed by the neighboring lipid chains. Thus, we confirmed that water in the DPhPC membrane has low mobility in any direction and a low probability of forming water clusters in the

TABLE 2: Excess Hydrational Free Energy of Test Molecules[a]

	H_2O	NH_3	O_2	CO	NO	CO_2	$CHCl_3$
$\mu_{ex}^{NPT}(R_{cav} = 2.6Å)$	-8.1 ± 0.6	-2.8 ± 0.2	2.50 ± 0.03	2.82 ± 0.04	1.96 ± 0.04	-0.02 ± 0.12	0.8 ± 2.1
$\mu_{ex}^{NPT}(R_{cav} = 2.7Å)$	-8.6 ± 0.6	-2.6 ± 0.2	2.50 ± 0.04	2.85 ± 0.06	1.97 ± 0.04	-0.02 ± 0.06	0.7 ± 1.5
$\mu_{ex}^{NPT}(R_{cav} = 2.8Å)$	-7.7 ± 0.7	-2.5 ± 0.1	2.53 ± 0.02	2.85 ± 0.06	1.99 ± 0.04	-0.06 ± 0.15	0.0 ± 0.7
$\mu_{ex}^{NPT}(R_{cav} = 2.9Å)$	-7.9 ± 0.7	-2.6 ± 0.1	2.49 ± 0.02	2.81 ± 0.02	1.94 ± 0.02	-0.08 ± 0.11	0.1 ± 0.9
μ_{ex}^{NPT}(average)	-8.1	-2.6	2.51	2.84	1.97	-0.05	0.5

[a] Units are in kcal/mol.

membrane interior. All these observations are quite consistent with the conjecture on the water behavior inside the membrane made on the basis of the cavity distribution. Again, these findings will partly account for the fact that chain branching leads to a greater reduction in the proton permeation rate than in the water permeation rate.

4. Conclusions

A comparative simulation of the straight-chained DPPC and branch-chained DPhPC bilayers was performed to assess the permeability of small neutral molecules in each. A series of excess chemical potential calculations of various neutral molecules demonstrated that lipid chain branching did not significantly change their partition coefficients between water and the hydrophobic membrane interior. However, analysis of cavity distribution in each bilayer system revealed that the branch-chained DPhPC molecules were better able to prevent large cavities from forming in their bilayer than were DPPC molecules. This suggested more restricted motion of small penetrants inside the branch-chained lipid bilayers. From an anaylsis of local diffusion coefficients of water, it was found that water molecules have considerably reduced mobility in the DPhPC membrane interior as compared with the DPPC membrane interior. This lower water mobility would be correlated with the lower mobility of the branched DPhPC chains. Thus, we conclude that the effects of chain branching on permeability are attributable mainly to the alteration in chain mobility, as far as the small neutral penetrants are concerned. As a result of reduced water diffusion in the branch-chained membrane, the water permeability of the DPhPC bilayer was less than that of the DPPC bilayer by about 30%. Furthermore, it is speculated that proton-wire type[2,44,46] conduction of protons in the branch-chained membrane may be significantly reduced due to the low probability of the water cluster formation in the membrane.

Acknowledgment. This work was supported in part by NAREGI Nanoscience Project, Ministry of Education, Culture, Sports, Science and Technology, Japan.

Appendix

To check the R_{cav} dependency of the calculated excess chemical potentials, we carried out the cavity insertion calculation for a series of small molecules in a pure water system. For this purpose, we first performed an NPT-MD run of a 512 TIP3P water system for 1 ns. The detail conditions are the same as those in the case of the lipid bilayer. We then calculated the excess chemical potentials by the cavity insertion technique with minimum radii R_{cav} of 2.6, 2.7, 2.8, and 2.9 Å, respectively. In each case, 2 million trial insertions were performed, and this procedure was conducted for a total of 10 times. The calculated excess chemical potentials are listed in Table 2. The errors shown in the table denote the standard deviations of the repeated calculations. The results indicated that, first of all, there was no obvious R_{cav} value dependence of the excess chemical potential in any of the test cases: the discrepancy due to the different R_{cav} values was within the statistical margin of error. Nonpolar molecules (O_2, CO, NO, CO_2) generally showed good convergence, though a large carbon dioxide molecule showed a relatively large statistical error. Polar molecules gave less accurate chemical potentials because of a complex charge interaction in an aqueous environment. Since the statistical error for $CHCl_3$ was too large to provide a quantitative evaluation of the hydration excess free energy, we should limit our discussion to a qualitative comparison with respect to the chemical potential of $CHCl_3$.

References and Notes

(1) Guyton, A. C.; Hall, J. E. *Textbook of Medical Physiology*; W. B. Saunders: Philadelphia, 1996.
(2) *Permeability and Stability of Lipid Bilayers*; Disalvo, E. A.; Simon, S. A., Eds.; CRC Press: Boca Raton, FL, 1995.
(3) *The Structure of Biological Membranes*; Yeagle, P., Ed.; CRC Press: Boca Raton, FL, 1991.
(4) Jansen, M.; Blume, A. *Biophys. J.* **1995**, *68*, 997.
(5) Mathai, J. C.; Sprott, G. D.; Zeidel, M. L. *J. Biol. Chem.* **2001**, *276*, 27266.
(6) Yamauchi, Y.; Doi, K.; Kinoshita, M.; Kii, F.; Fukuda, H. *Biochim. Biophys. Acta* **1992**, *1110*, 171. Yamauchi, K.; Doi, K.; Yoshida, Y.; Kinoshita, M. *Biochim. Biophys. Acta* **1993**, *1146*, 178.
(7) Taylor, R. J.; de Levie, R. *Biophys. J.* **1991**, *59*, 873.
(8) Baba, T.; Minamikawa, H.; Hato, M.; Handa, T. *Biophys. J.* **2001**, *81*, 3377.
(9) Fettiplace, R. *Biochim. Biophys. Acta* **1978**, *513*, 1. Olbrich, K.; Rawicz, W.; Needham, D.; Evans, E. *Biophys. J.* **2000**, *79*, 321.
(10) Schatzberg, P. *J. Polym. Sci. C.* **1965**, *10*, 87.
(11) Shinoda, W.; Mikami, M.; Baba, T.; Hato, M. *J. Phys. Chem. B.* **2003**, *107*, 14030.
(12) Jedlovszky, P.; Mezei, M. *J. Am. Chem. Soc.* **2000**, *122*, 5125.
(13) Nagle, J. F.; Zhang, R.; Tristram-Nagle, S.; Sun, W.; Petrache, H. I.; Suter, R. M. *Biophys. J.* **1996**, *70*, 1419.
(14) MacKerell, A. D., Jr.; Bashford, D.; Bellott, M.; Dunbrack R. L., Jr.; Evanseck, J. D.; Field, M. J.; Fischer, S.; Gao, J.; Guo, H.; Ha, S.; Joseph-McCarthy, D.; Kuchnir, L.; Kuczera, K.; Lau, F. T. K.; Mattos, C.; Michnick, S.; Ngo, T.; Nguyen, D. T.; Prodhom, B.; Reiher, W. E., III; Roux, B.; Schlenkrich, M.; Smith, J. C.; Stote, R.; Straub, J.; Watanabe, M.; Wiorkiewicz-Kuczera, J.; Yin, D.; Karplus, M. *J. Phys. Chem. B* **1998**, *102*, 3586.
(15) Jorgensen, W. L.; Chandrashekar, J.; Madura, J. D.; Impey, R.; Klein, M. L. *J. Chem. Phys.* **1983**, *79*, 926.
(16) Husslein, T.; Newns, D. M.; Pattnaik, P. C.; Zhong, Q.; Moore, P. B.; Klein, M. L. *J. Chem. Phys.* **1998**, *109*, 2826.
(17) Marrink, S. J.; Sok, R. M.; Berendsen, H. J. C. *J. Chem. Phys.* **1996**, *104*, 9090.
(18) Li, H.; Elber, R.; Straub, J. E. *J. Biol. Chem.* **1993**, *268*, 17908.
(19) Somasundaram, T.; Panhuis, M. I. H.; Lynden-Bell, R. M.; Patterson, C. H. *J. Chem. Phys.* **1999**, *111*, 2190.
(20) Jorgensen, W. L.; Briggs, J. M.; Contreras, M. L. *J. Phys. Chem.* **1990**, *94*, 1683.
(21) Martyna, G. J.; Tuckerman, M. E.; Klein, M. L. *J. Chem. Phys.* **1992**, *97*, 2638.
(22) Martyna, G. J.; Tobias, D. J.; Klein, M. L. *J. Chem. Phys.* **1994**, *101*, 4177.
(23) Martyna, G. J.; Tuckerman, M. E.; Tobias, D. J.; Klein, M. L. *Mol. Phys.* **1996**, *87*, 1117.
(24) Brooks, B. R.; Bruccoleri, R. E.; Olafson, B. D.; States, D. J.; Swaminathan, S.; Karplus, M. *J. Comput. Chem.* **1983**, *4*, 187.
(25) We, Y.; He, K.; Ludtke, S. J.; Huang, H. W. *Biophys. J.* **1995**, *68*, 2361.
(26) Frenkel, D.; Smit, B. *Understanding of Molecular Simulation*, 2nd ed.; Academic Press: San Diego, 2002.

(27) Deitric, G. L.; Scriven, L. E.; Davis, H. T. *J. Chem. Phys.* **1989**, *90*, 2370.
(28) Pohorille, A.; Wilson, M. A. *J. Chem. Phys.* **1996**, *104*, 3760.
(29) Marrink, S. J.; Berendsen, H. J. C. *J. Phys. Chem.* **1994**, *98*, 4155.
(30) Ryckaert, J. P.; Ciccotti, G.; Berendsen, H. J. C. *J. Comput. Phys.* **1977**, *23*, 327.
(31) Kawakami, T.; Aizawa, K.; Okazaki, S., private communication.
(32) Allen, M. P.; Tildesley, D. J. *Computer Simulation of Liquids*; Clarendon Press: Oxford, U.K., 1987.
(33) Ulander, J.; Haymet, A. D. J. *Biophys. J.* **2003**, *85*, 3475.
(34) Shinoda, W.; Shimizu, M.; Okazaki, S. *J. Phys. Chem. B* **1998**, *102*, 6647.
(35) van Gunsteren, W. F.; Berendsen, H. J. C. Groningen Molecular Simulation (GROMOS); software package, Biomos, Nijenborgh 4, 9747 AG Groningen, The Netherlands.
(36) Berendsen, H. J. C.; Postma, J. P. M.; van Gunsteren, W. F.; Hermans, J. In *Intermolecular Forces*; Pullman, B., Ed.; Reidel: Dordrecht, Germany, 1981; pp 331−342.
(37) Gennis, R. B. *Biomembranes: Molecular Structure and Function*; Springer-Verlag: Berlin, 1989.
(38) Ligeza, A.; Tikhonov, A. N.; Hyde, J. S.; Subczynski, W. K. *Biochim. Biophys. Acta* **1998**, *1365*, 453.
(39) Forster, R. E.; Gros, G.; Lin, L.; Ono, Y.; Wunder, M. *Proc. Natl. Acad. Sci. U.S.A.* **1998**, *95*, 15821.
(40) Strictly speaking, in the NPT ensemble, the molecular dynamics does not obey the correct Newtonian dynamics. However, the calculated diffusion coefficient was almost identical with that obtained in micro-canonical ensemble: the difference was well within the statistical error. We have confirmed this by analysis of a 10 ns-NVE MD trajectory.
(41) Bacic, G.; Srejic, R.; Ratkovic, S. *Stud. Biophys.* **1990**, *138*, 95.
(42) Lawaczeck, R. *J. Membrane Biol.* **1979**, *51*, 229.
(43) Carruthers, A.; Melchior, D. L. *Biochemistry* 1983, 22, 5797.
(44) Paula, S.; Volkov, A. G.; van Hoek, A. N.; Haines, T. H.; Deamer, D. W. *Biophys. J.* **1996**, *70*, 339.
(45) Negrete, H. O.; Rivers, R. L.; Gough, A. H.; Colombini, M.; Zeidel, M. L. *J. Biol. Chem.* **1996**, *271*, 11627.
(46) Nagle, J. F. J. *Bioenerg. Biomembr.* **1987**, *19*, 413.
(47) Marrink, S. J.; Jähnig, F.; Berendsen, H. J. C. *Biophys. J.* **1996**, *71*, 632.
(48) Venable, R. M.; Pastor, R. W. *J. Chem. Phys.* **2002**, *116*, 2663.